Single-crystal neutron diffraction study of hexagonal multiferroic $YbMnO_3$ under a magnetic field

S. Chattopadhyay,[1,2,*] V. Simonet,[3] V. Skumryev,[4,5] A. A. Mukhin,[6] V. Yu. Ivanov,[6] M. I. Aroyo,[7] D. Z. Dimitrov,[8,9] M. Gospodinov,[8] and E. Ressouche[1]

[1]*Université Grenoble Alpes, INAC-MEM, 38000 Grenoble, France*

[2]*Dresden High Magnetic Field Laboratory (HLD-EMFL), Helmholtz-Zentrum Dresden-Rossendorf, 01328 Dresden, Germany*

[3]*Institut Néel, CNRS and Université Grenoble Alpes, BP 166, 38000 Grenoble, France*

[4]*Departament de Física, Universitat Autònoma de Barcelona, 08193 Bellaterra, Barcelona, Spain*

[5]*Institució Catalana de Recerca i Estudis Avançats, 08010 Barcelona, Spain*

[6]*Prokhorov General Physics Institute, Russian Academy of Sciences, 119991 Moscow, Russia*

[7]*Department of Condensed Matter Physics, University of the Basque Country UPV/EHU, Apartado 644, 48080 Bilbao, Spain*

[8]*Institute of Solid State Physics, Bulgarian Academy of Sciences, 1184 Sofia, Bulgaria*

[9]*Institute of Optical Materials and Technologies, Bulgarian Academy of Sciences, 1113 Sofia, Bulgaria*

(Received 29 May 2018; revised manuscript received 21 August 2018; published 9 October 2018)

We report a single-crystal neutron diffraction study of the magnetic structure of the multiferroic compound $YbMnO_3$, a member of the hexagonal manganite family, in zero field and under a magnetic field applied along the c axis. We propose a scenario for the zero-field magnetic ordering and for the field-induced magnetic reorientation of the Mn atom and of the two Yb atoms on distinct crystallographic sites, compatible with the macroscopic measurements, as well as with previous powder neutron diffraction experiments and results from other techniques (optical second-harmonic generation and Mössbauer spectroscopy). Our study should contribute to settling some debated issues regarding the magnetic properties of this material as part of a broader investigation of the entire hexagonal $RMnO_3$ (R = Dy, Ho, Er, Tm, Yb, Lu, Y) family.

DOI: 10.1103/PhysRevB.98.134413

I. INTRODUCTION

The hexagonal h-$RMnO_3$ multiferroic compounds (with R = Dy, Ho, Er, Tm, Yb, Lu, Y) have been the subject of an abundant amount of literature since their discovery in 1963 [1]. This interest is due to their exotic static and dynamical behaviors ascribed to the combination of ferroelectricity and magnetic frustration. The latter arises from the intraplane triangular arrangement of antiferromagnetically interacting Mn^{3+} magnetic ions, weakly coupled along the c axis, as shown in Fig. 1. Unlike multiferroics, where the ferroelectricity is induced by the magnetic order, as in the orthorhombic $RMnO_3$ compounds (with larger rare-earth ions), h-$RMnO_3$ oxides become ferroelectric at much higher temperatures (around 1000 K) than their magnetic transition (Néel temperature T_N below 100 K). In h-$YMnO_3$, ferroelectricity was found to be connected to the buckling of the layered MnO_5 polyhedra, displacements of the Y ions, and the trimerization of the Mn lattice associated with strong magnetoelastic effects [2–9]. Although the exact mechanism at the origin of the ferroelectricity has been debated, it is assumed to be identical in all members of the family, which are described in the hexagonal space group $P6_3cm$ (number 185) at low temperature.

The magnetism is a complex issue in itself in this class of materials. Mn^{3+} ions occupy the Wyckoff site 6c, forming triangular layers of Mn^{3+} in the (a, b) planes. Between them, R^{3+} occupies two different crystallographic Wyckoff sites, 4b and 2a. While decreasing the temperature, first the Mn^{3+} order magnetically at T_N due to superexchange antiferromagnetic interactions in a 120° magnetic structure, characterized by a $k = (0, 0, 0)$ propagation vector [1], and then R^{3+} (4b) are polarized in the molecular field of the Mn, while R^{3+} (2a) are believed to order at much lower temperature from their mutual interactions [10]. Additional spin reorientations occur at intermediate temperatures for some members of the family (e.g., Ho, Sc). Finally, metamagnetic processes are frequently observed under magnetic field. Magnetoelectric coupling is also evidenced by strong dielectric anomalies visible at each magnetic transition [11]. The major tools that have been used to determine the various magnetic configurations of h-$RMnO_3$ are neutron diffraction and optical second-harmonic generation (SHG). They often, but not always, agree. For the unpolarized neutron scattering method, difficulties arise from the indetermination among different possible magnetic structures (homometric pairs) [12], whereas the SHG technique has difficulty distinguishing different magnetic sublattices. In addition, neutron scattering has often been performed only on polycrystalline samples, which is usually not sufficient to determine field-induced magnetic structures.

In this paper, we concentrate on $YbMnO_3$, which was reported to undergo a magnetic transition below $T_N \sim 80$ K with a propagation vector $k = (0, 0, 0)$ [10,13]. Powder neutron diffraction [14] and SHG [15,16] agree on the high-temperature magnetic ordering. However, the interpretation of the low-temperature magnetic configuration, in particular

*s.chattopadhyay@hzdr.de

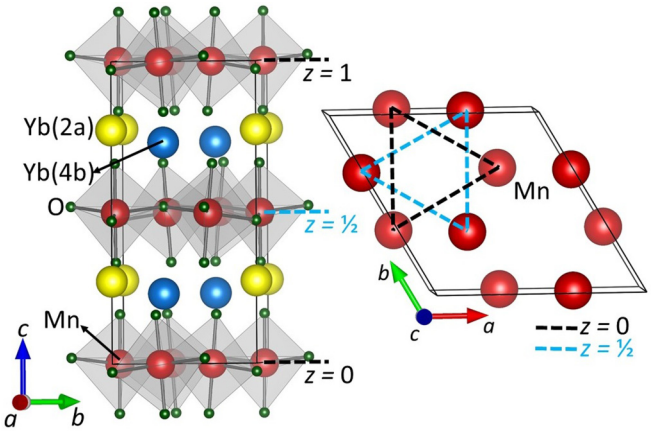

FIG. 1. Left: Perspective view of the $YbMnO_3$ crystal structure with tilted MnO_5 bi-pyramids and Yb atoms on the different 4*b* and 2*a* Wyckoff sites, respectively (the small green spheres are oxygen atoms). Right: Two layers of Mn triangles positioned at $z = 0$ and $z = 1/2$ along the crystallographic *c* direction.

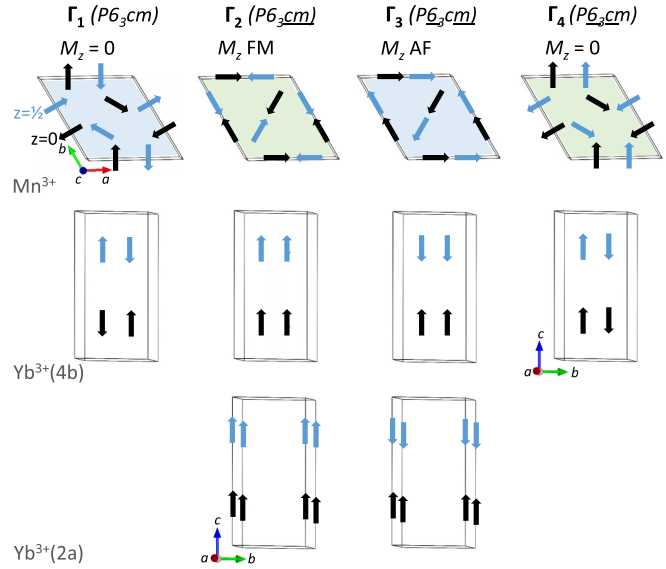

FIG. 2. Magnetic structures associated with the one-dimensional irreducible representations of $P6_3cm$ ($k = 0$) for Mn^{3+}, Yb^{3+} (4*b*), and Yb^{3+} (2*a*), shown in the top, middle, and bottom panels, respectively. The corresponding isotropy magnetic groups are also indicated. The Mn homometric pairs are indicated by similar colors. The magnetic moments in the $z = 0$ and $z = 1/2$ planes are shown in black and blue, respectively. For Mn^{3+}, the *z* component of the magnetic moment with its ferromagnetic (FM) or antiferromagnetic (AF) coupling is also indicated.

when Yb (2*a*) atoms are expected to play a role, is not clear, and neither are the exact mutual orientations of the three magnetic ions under magnetic field. Moreover, hysteretic effects, the coexistence of competing phases even in zero field or a spin reorientation at intermediate temperature, have also been reported [16–18], justifying the necessity of a single-crystal neutron diffraction experiment on this composition.

II. SYNTHESIS AND EXPERIMENTAL DETAILS

The platelike single crystals of $YbMnO_3$, with the hexagonal *c* axis perpendicular to the surface and a thickness of about 0.5 mm, were grown using the flux method as described by Yen *et al.* [19]. The magnetization *M* measurements were performed in a commercial superconducting quantum interference device magnetometer and in a physical property measurement system from Quantum Design. Electric polarization *P* was measured along the crystallographic *c* axis using a Keithley 6517A electrometer. Electrical contacts were attached by Ag paint to the two parallel surfaces of the *c*-cut sample. The measurements were performed for both zero and nonzero (± 1 kV/mm) applied electric field regimes. These have not revealed a significant difference, implying the absence of Ohmic currents. Note that the latter were observed in $YMnO_3$ at temperatures above 230 K and were accompanied by a negative magnetoresistive effect [20]. No preliminary poling was carried out to polarize the sample possessing a ferroelectric domain structure. Neutron diffraction measurements in zero magnetic field were performed on the CEA-CRG D15 and D23 single-crystal diffractometers at the Institut Laue-Langevin (ILL; wavelengths $\lambda = 1.173$ and 1.27 Å, respectively) in the four-circle mode using a standard orange cryostat. The CEA-CRG D23 diffractometer at the ILL was also used for the measurements under magnetic field using a lifting-arm detector and a vertical cryomagnet. The zero-field measurements on D15 and D23 were determined to be consistent, and only results from D23 are presented in the following.

III. IRREDUCIBLE REPRESENTATION ANALYSIS

Let us recall that group theory and representation analysis [21] reveal that the representation of the magnetic structure for Mn^{3+} and Yb^{3+} (4*b*) involve six possible irreducible representations (IRs), denoted as Γ_i ($i = 1, 2, \ldots, 6$), which are compatible with the $P6_3cm$ space group and the propagation vector $k = (0, 0, 0)$ [22]. Four of these, Γ_1 to Γ_4, are unidimensional and are depicted in Fig. 2, with the last two being two-dimensional. For the Yb^{3+} (2*a*) site, only the Γ_2, Γ_3, Γ_5, and Γ_6 irreducible representations are allowed.

Concerning the Mn^{3+} site, the magnetic moments are constrained in the (a, b) plane for Γ_1 and Γ_4, while an out-of-plane ferromagnetic component is allowed for Γ_2 and an out-of-plane antiferromagnetic component is allowed for Γ_3. Among these configurations, those with symmetries Γ_1 and Γ_3 correspond to homometric pairs, and so do Γ_2 and Γ_4. This means that these pairs are hardly distinguishable (almost identical intensities of the magnetic Bragg reflections) by neutron diffraction when the Mn^{3+} coordinate x_{Mn} is close to 1/3. For the two-dimensional representations Γ_5 and Γ_6, the Fourier components of the magnetic moments are written as a linear combination of six basis functions. The corresponding magnetic structures are reported in Ref. [22]. For Γ_5, there are four magnetic modes with the magnetic moments in the (a, b) plane, displaying either a ferromagnetic or a 120° arrangement. The coupling is ferromagnetic between the planes. The two other modes are discarded since they concern nonequal moments along the *c* axis. Similar solutions are found for Γ_6 but with an antiferromagnetic coupling of the in-plane magnetic structures along the *c* axis. Concerning the Yb^{3+}(4*b*)

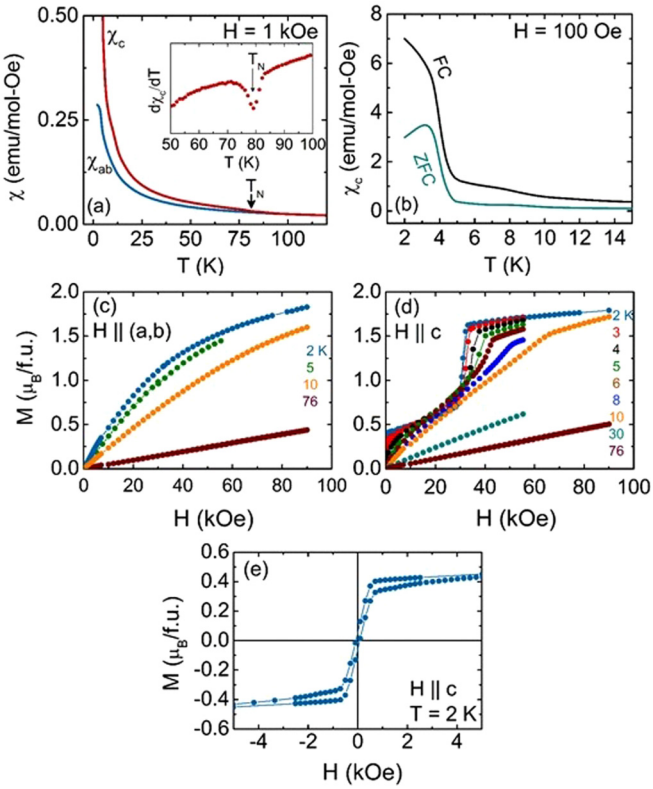

FIG. 3. (a) The dc magnetic susceptibility χ along the c axis and in the (a, b) plane. Measurements were performed in a magnetic field of 1 kOe on cooling. Inset: $\frac{d\chi_c}{dT}$ vs T to show the transition at $T_N =$ 80 K. (b) $\chi(T)$ measured with a field of 100 Oe along the c axis after field-cooling and zero-field-cooling procedures, showing the low-temperature anomaly associated with the Yb^{3+} $(2a)$ ordering. Magnetization M vs applied magnetic field H for H in the (a, b) plane (c) and along c (d). (e) The low-field $M(H)$ curve at 2 K for $H \parallel c$. The data are not corrected for the demagnetizing field effect.

and $Yb^{3+}(2a)$ sites, the one-dimensional IRs correspond to magnetic moments along the c axis. Importantly, only the Γ_2 configuration allows a ferromagnetic component along the c axis for the three sites (see Fig. 2).

IV. RESULTS

A. Magnetization and electric polarization

Figure 3(a) depicts the temperature T variation of the dc magnetic susceptibility χ in a magnetic field of 1 kOe along the c direction (χ_c) and within the (a, b) plane (χ_{ab}), recorded on cooling. An anisotropic response is seen, apparently below the Néel temperature, with the χ_c/χ_{ab} ratio value reaching ~15 at 2 K. The data well replicate the results reported in previous studies [10,13,14,19,23]. The anomaly near 80 K (T_N) in the χ_c data [inset of Fig. 3(a)] corresponds to the ordering of Mn^{3+} magnetic moments, as reported earlier. The sharp increase in χ_c below about 5 K [Fig. 3(b)] signals the onset of long-range ordering of the Yb^{3+} $(2a)$ moments. The differences in the zero-field- and field-cooled thermomagnetic

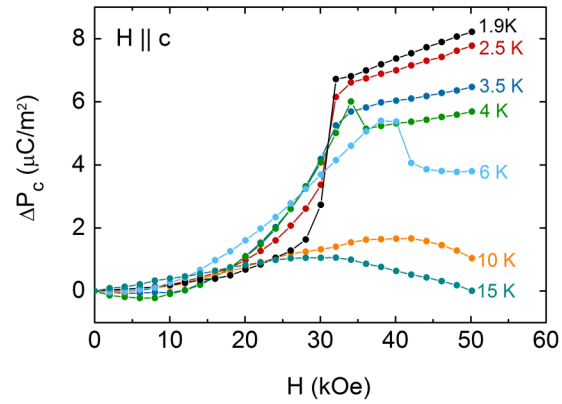

FIG. 4. Change in electric polarization ΔP_c along the c axis as a function of magnetic field H applied along the same direction (measured in an applied electric field of 1 kV/mm).

curves below about 4 K reflect the existence of net magnetic moment and coercivity.

The field dependence of the magnetization for various temperatures is shown in Figs. 3(c) and 3(d) for fields applied perpendicular and parallel to the c axis, respectively, and is again consistent with previous reports [10,19,24–26]. No anomaly or hysteretic behavior is measured for the magnetic field applied in the (a, b) plane. This is at variance with the behavior observed for the other orientation of the field where two steplike features are visible in the magnetization curve at low temperature. The low-field magnetization step is observed only for temperatures below about 5 K. As seen on the 2 K curve [Fig. 3(e)], the magnetization reaches $\sim 0.4\mu_B$/f.u. almost instantly after the magnetic field is increased (as soon as the applied field reaches $H_{c1} \sim 300$ Oe, which means that the internal field is even smaller). The magnetization step value and the magnetization hysteresis seen in Fig. 3(e) point to ferrimagnetic alignment between Yb^{3+} $(4b)$ and Yb^{3+} $(2a)$ moments. The second steplike anomaly appears near $H_{c2} = 30$ kOe for the 2 K curve. At this field, a jump in magnetization takes place, and it increases with about $1.2\,\mu_B$/f.u. above its low-field step value of $\sim 0.4\mu_B$/f.u. and becomes closer to the (a, b) plane magnetization. This steplike feature actually reveals a *field-induced* spin reorientation that is addressed through our neutron diffraction measurements presented below. It smears out with increasing temperature along with the shift of H_{c2} towards higher field.

The field dependence of the electric polarization change $\Delta P_c(H)$ along the c axis is presented in Fig. 4 for several temperatures. The magnetic field was applied along the same direction. A sharp jump in the polarization is observed at ~30 kOe at the lowest temperatures. It is clearly correlated to the field-induced magnetic phase transition since its threshold field coincides with the second steplike anomaly in the magnetization curves at H_{c2}. The polarization anomaly smears out with increasing temperature. Its field dependence changes character between $T_c \sim 4$ and 6 K, revealing a broad maximum in $\Delta P_c(H)$ at higher temperatures. These modifications are probably associated with a change in the nature of the field-induced transition above and below the Yb^{3+} $(2a)$ ordering at T_c.

TABLE I. Results of the refinement of the single-crystal neutron diffraction Bragg peak intensities recorded above (100 K) and below (30, 13, and 2 K) the transition temperature ($T_N = 80$ K) under the zero-magnetic-field condition. R_F, R_{F^2}, and R_{F^2w} are the agreement factors of the fits [27], M is the magnetic moment, and x_{Mn} is the x coordinate of Mn^{3+}.

$T = 100$ K, $x_{\mathrm{Mn}} = 0.3345(20)$	
($R_F = 4.7\%$, $R_{F^2} = 5.5\%$, $R_{F^2w} = 6.3\%$)	
$T = 30$ K, $x_{\mathrm{Mn}} = 0.3343(14)$	
($R_F = 3.8\%$, $R_{F^2} = 5.3\%$, $R_{F^2w} = 6.0\%$)	
Ion/IR	M (units of μ_B)
Mn^{3+}/Γ_4	3.32(3)
Yb^{3+} ($4b$)/Γ_4	0.81(5)
$T = 13$ K, $x_{\mathrm{Mn}} = 0.3350(15)$	
($R_F = 3.9\%$, $R_{F^2} = 5.3\%$, $R_{F^2w} = 6.4\%$)	
Ion/IR	M (units of μ_B)
Mn^{3+}/Γ_4	3.41(4)
Yb^{3+} ($4b$)/Γ_4	1.15(5)
$T = 2$ K, $x_{\mathrm{Mn}} = 0.3349(15)$	
($R_F = 3.5\%$, $R_{F^2} = 4.9\%$, $R_{F^2w} = 6.2\%$)	
Ion/IR	M (units of μ_B)
Mn^{3+}/Γ_2	3.41(3)
Yb^{3+} ($4b$)/Γ_2	1.76(7)
Yb^{3+} ($2a$)/Γ_2	−1.47(8)

B. Single-crystal neutron diffraction

1. In zero magnetic field

About 700 Bragg reflections were recorded at 100, 30, 13, and 2 K [the magnetic Bragg peaks associated with the $k = (0, 0, 0)$ propagation vector rise above the nuclear ones]. All the refinements were performed using the FULLPROF SUITE software package [27], and we used the formalism of Becker-Coppens to refine the anisotropic extinction [28]. The refined atomic positions of the 100 K data (above T_N) were found to be very similar to the ones reported from x-ray diffraction at room temperature [29,30]. In particular, the z coordinate of Mn^{3+} is almost zero and is thus kept to zero for the lower-temperature refinements. The x coordinate of Mn^{3+} x_{Mn} is very close to 1/3 (see Table I), but it was allowed to vary in the lower-temperature refinements as its variation is believed to be intricately linked to the selection of the magnetic order [31].

To get deeper insight into the contribution of the different sublattices to the magnetic order in zero field, we chose to study the thermal evolution of some characteristic site-specific reflections (see Fig. 5). We followed the (1, 0, 1) and (1, 0, 3) reflections, which are forbidden in the $P6_3cm$ space group. As can be seen, they start to become nonzero only below T_N, reflecting their magnetic character, and have a temperature dependence compatible with that of a magnetic order parameter. Under Γ_2 and Γ_4 symmetry, those two reflections are entirely dependent on the ordering of Mn^{3+} magnetic moments. Therefore, the rise of these reflections below T_N is consistent with the coincidence of the Néel temperature with the magnetic ordering of Mn^{3+} in one of these two IRs. In contrast, the $(-1, 0, 0)$ reflection shown in Fig. 5(e) depends, for its magnetic component, only on the Yb^{3+} magnetic

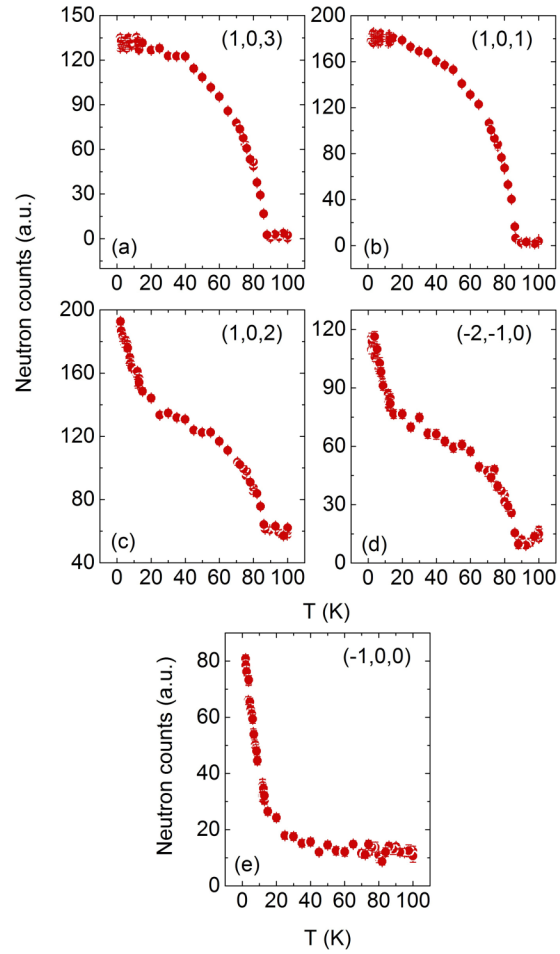

FIG. 5. Neutron counts at the peak maximum versus temperature for three types of Bragg reflections. They are site specific for the magnetic arrangements corresponding to Γ_2 and Γ_4: (a) and (b) (1, 0, 3) and (1, 0, 1) contributed solely by ordered Mn^{3+}, (c) and (d) (1, 0, 2) and $(-2, -1, 0)$ contributed by all Mn^{3+}, Yb^{3+} ($4b$), and Yb^{3+} ($2a$), and (e) $(-1, 0, 0)$ contributed solely by Yb^{3+} ($4b$) and Yb^{3+} ($2a$). Note that the Γ_4 configuration is not allowed by symmetry for the Yb^{3+} ($2a$) magnetic order.

moments for Γ_2 ($2a$ and $4b$ sites) and Γ_4 (only the $4b$ site). The intensity of this reflection increases very slowly when decreasing the temperature down to ∼20−30 K, below which it shows a sharp increment. Such behavior is consistent with the magnetic ordering of Yb^{3+} ($4b$) in the Mn^{3+} molecular field [14]. Note that, as the transition at T_N is second order, the two Mn^{3+} and Yb^{3+} ($4b$) sublattices must order with the same IR (Γ_2 or Γ_4) since they are coupled. No anomaly can be seen in $(-1, 0, 0)$ at T_c. Two other characteristic reflections, viz., (1,0,2) and $(-2, -1, 0)$, combine the features of the previous two kinds of reflections, thus involving magnetic contributions from both Mn^{3+} and Yb^{3+}.

We checked the information deduced from the temperature dependence of selected reflections through the refinement of all the Bragg reflections below T_N. To obtain the best refinements, all the possible one-dimensional IRs predicted for Mn^{3+} and Yb^{3+} were tested. In addition to the magnitude of the magnetic moments, the x coordinate of the Mn^{3+} ions was also refined. At 30 and 13 K, the best refinements with

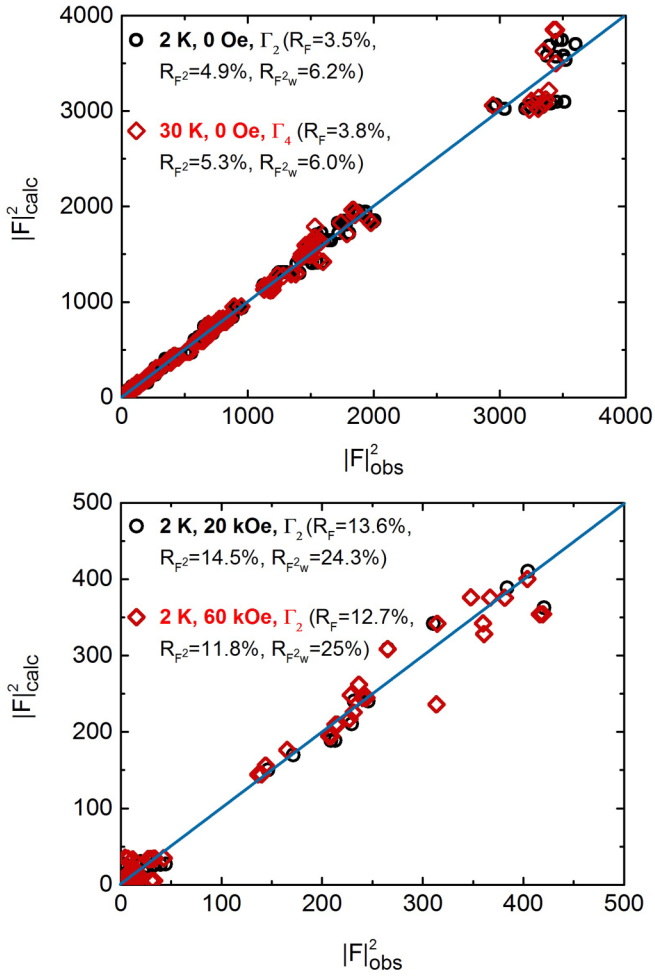

FIG. 6. Observed versus calculated intensity (square of the structure factor) of the magnetic Bragg reflections in arbitrary units. Top: Data recorded in zero field at $T = 30$ K (red diamonds) and 2 K (black circles) using the four-circles mode. Bottom: Data recorded at $T = 2$ K with $H = 20$ kOe (black circles) and 60 kOe (red diamonds) in the cryomagnet using the lifting-arm detector. The agreement factors and magnetic configurations for the three sites are indicated.

similar agreement factors were obtained for representations Γ_4 and Γ_2 for Mn^{3+}/Yb^{3+} ($4b$) (homometric Mn^{3+} IR), with an enhancement of the Yb^{3+} ($4b$) moment from 30 to 13 K and no magnetic moment on the Yb^{3+} ($2a$) sites. However, in the Γ_2 magnetic configuration, the Yb^{3+} ($4b$) are ferromagnetically coupled. From the neutron refinement, they should give rise to a ferromagnetic contribution amounting to $\sim 0.7\mu_B$ at 30 K and $\sim 0.9\mu_B$ at 13 K, which is not observed in the magnetization measurements. A small bifurcation of the field-cooled and zero-field-cooled susceptibilities has been reported [13] below T_N, but it cannot be accounted for by such a large magnetization and is rather due to field-polarized defective magnetic moments, for instance, in the domain walls [19]. Our finding thus points to the Γ_4 magnetic configuration for Mn^{3+} and Yb^{3+} ($4b$) (see Figs. 6 and 7), which is consistent with previous powder neutron diffraction [14] and SHG results [15]. The good quality of the fits obtained using Γ_4/Γ_2 configurations allowed us to limit our analysis to solutions corresponding to one-dimensional IRs over the more complex two-dimensional ones.

Mössbauer and far-infrared spectroscopies have proven the ordering of the Yb^{3+} ($2a$) below ~ 5 K [14,32,33]. Moreover, the onset of a ferromagnetic component along the c axis is associated with this ordering, which suggests that the Yb^{3+} ($2a$) moments order in the Γ_2 IR. The last uncertainty concerns the ordering of Mn^{3+} and Yb^{3+} ($4b$) below T_c. Do they remain in the Γ_4 IR, or do they reorient due to a coupling with the Yb^{3+} ($2a$) in the Γ_2 IR? We checked both possibilities: Although the agreement factor is only slightly better for the Γ_2 solution for all sites versus the solution with Γ_4 for Mn^{3+} and Yb^{3+} ($4b$) and Γ_2 for Yb^{3+} ($2a$), the former is more consistent with the magnetization data, yielding almost $0.5\,\mu_B$/f.u., as shown in Fig. 3(d). Indeed, the total ferromagnetic component deduced from the neutron refinement for the Γ_2 solution is found to be equal to $0.68(8)\mu_B$/f.u., instead of $0.06(3)\mu_B$ obtained for the Γ_4/Γ_2 solution. We have also tested the possibility of an in-plane configuration of Yb^{3+} ($2a$) magnetization that had been suggested [14] but found worse agreement with our data. The results of the fits are shown in Fig. 6, with the associated magnetic configuration given in Fig. 7, and the details of the important refined parameters are given in Table I.

2. *Under magnetic field*

Figure 8 depicts the magnetic field dependence of characteristic reflections measured at 1.5 and 4.5 K, i.e., below and close to the transition T_c, with a field applied along the c axis. The results are identical: The $(1, 0, -1)$ [and also $(-2, 0, 1)$] reflection, which depends solely on Mn^{3+} under the Γ_2 IR, remains practically insensitive to the field sweep. On the other hand, the $(1, 0, 0)$ reflection, which is associated with Yb^{3+}($4b$) and Yb^{3+} ($2a$) magnetic moments in the Γ_2 IR, strongly decreases at 30 kOe and almost vanishes above this field. This field corresponds to H_{c2}, marking the high-field steplike anomaly observed in the macroscopic measurements for a field applied along the c axis. The last reflection, $(2, 1, 0)$, combines the two contributions from Mn^{3+} and from Yb^{3+}. It is therefore evident that only the Yb^{3+} moments are affected by the application of an external magnetic field.

Although nearly 140 reflections were recorded at 2 K for $H = 0.25$ kOe ($H < H_{c2}$) and 60 kOe ($H > H_{c2}$), the small coverage of the reciprocal space due to the limited aperture of the cryomagnet did not allow us to perform a reliable refinement of the data. Instead, we tested the most reasonable assumption agreeing with the magnetization data: a reorientation of the Yb^{3+} ($2a$) magnetic moments above H_{c2} in a way that they become parallel to the Yb^{3+} ($4b$) ones while keeping the Mn^{3+} magnetic moments unaltered in the (a, b) plane. This reorientation would lead, keeping the Yb^{3+} ($4b$) and Yb^{3+} ($2a$) magnetic moments at their absolute values refined in zero field, to a total magnetization per formula unit equal to $1.65\,\mu_B$, in agreement with the magnetization data of Fig. 3. As a starting point for the analysis of the data under field, we tested the magnetic configuration found previously in zero field using the four-circles mode. This configuration yields comparable agreement factors using the data recorded with the cryomagnet and lifting-arm detector in zero field and under a magnetic field of 20 kOe ($R_F/R_{F^2}/R_{F^2w}$

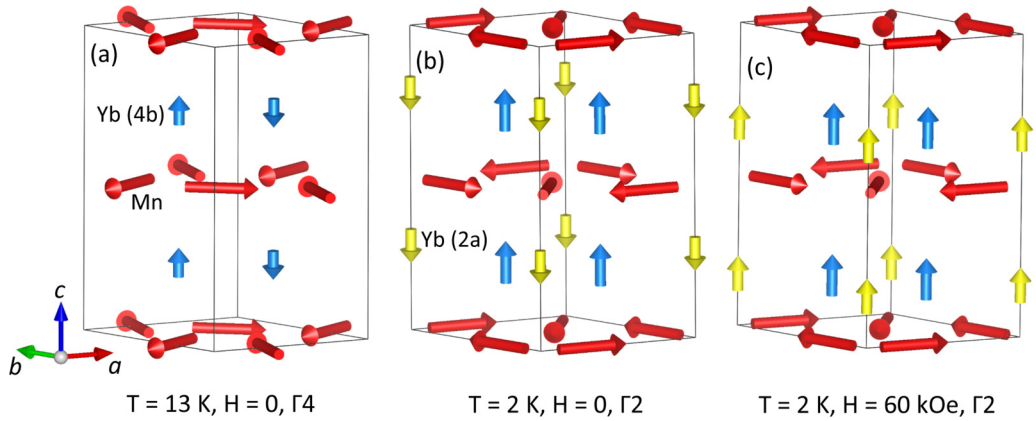

FIG. 7. Magnetic structures (and corresponding IR) refined in zero magnetic field at (a) 13 K and (b) 2 K. (c) Magnetic structure inferred from the neutron and magnetization data in a 60-kOe field at 2 K. The Mn^{3+} moments are represented in red, the Yb^{3+} (4*b*) in moments are blue, and the Yb^{3+} (2*a*) moments are in yellow.

$= 13.7\%/15.4\%/18.7\%$ and $13.6\%/14.5\%/24.3\%$, respectively). At 60 kOe, i.e., above H_{c2}, the same configuration does not hold well any longer, as evidenced by worse agreement factors ($R_F/R_{F^2}/R_{F^2w}$= 24.2%/17.9%/43.8%). Those improve significantly ($R_F/R_{F^2}/R_{F^2w} = 12.7\%/11.8\%/25\%$) by reversing the Yb^{3+} (2*a*) magnetic moments and making them parallel to the Yb^{3+} (4*b*) ones (see bottom panel of Fig. 6), hence validating the model. It should be noted that the strong decrease in the (1, 0, 0) Bragg reflection above H_{c2}, as depicted in Fig. 8, is obtained within this model (where all the Yb^{3+} magnetic moments are aligned along the field) due to the destructive interference between the two Yb^{3+} sublattices.

At 10 K ($T_c < T < T_N$) the same set of reflections was recorded at field values of 4 T and at 8 T, i.e., below and above the critical field corresponding to H_{c2} for this temperature [see Fig. 3(c)]. Again, a full refinement is impossible, but the data unambiguously show that the Yb^{3+} (4*b*) and Yb^{3+} (2*a*) moments order in the Γ_2 IR and are aligned parallel to each other and to the field for both values of the field. It is impossible to determine whether the Mn^{3+} magnetic moments are in Γ_2 or Γ_4. At 8 T, the data are compatible with the same configuration as the one inferred from the data at 2 K and 6 T which corresponds to the full polarization of the two Yb^{3+} sites. Note that the low-field phase with both Yb^{3+} moments antiparallel to each other does not seem to exist at 10 K.

C. Summary and discussion

In summary, we have achieved a good description of the magnetic properties of the h-$YbMnO_3$ compound through our single-crystal neutron diffraction study. We have found that the Mn^{3+} magnetic moments order below $T_N = 80$ K, polarizing the Yb^{3+} (4*b*) moments, whose ordered component strongly increases below 20–30 K. Both Mn^{3+} and Yb^{3+} (4*b*) moments are described with respect to Γ_4 in this temperature region. Below 5 K, the Yb^{3+} (2*a*) moments order in Γ_2, dragging Mn^{3+} and Yb^{3+} (4*b*) into a new kind of magnetic configuration also corresponding to Γ_2. It consists of a ferromagnetic arrangement of the Yb^{3+} (2*a*) and Yb^{3+} (4*b*) moments along *c* in a way that the Yb^{3+} (2*a*) and Yb^{3+} (4*b*) magnetic sublattices are antiparallel to each other. There happens also to be an important spin reorientation of the in-plane Mn^{3+} moments by 90°, as well as an additional change in its interlayer coupling from antiferromagnetic to ferromagnetic. Under a magnetic field applied along

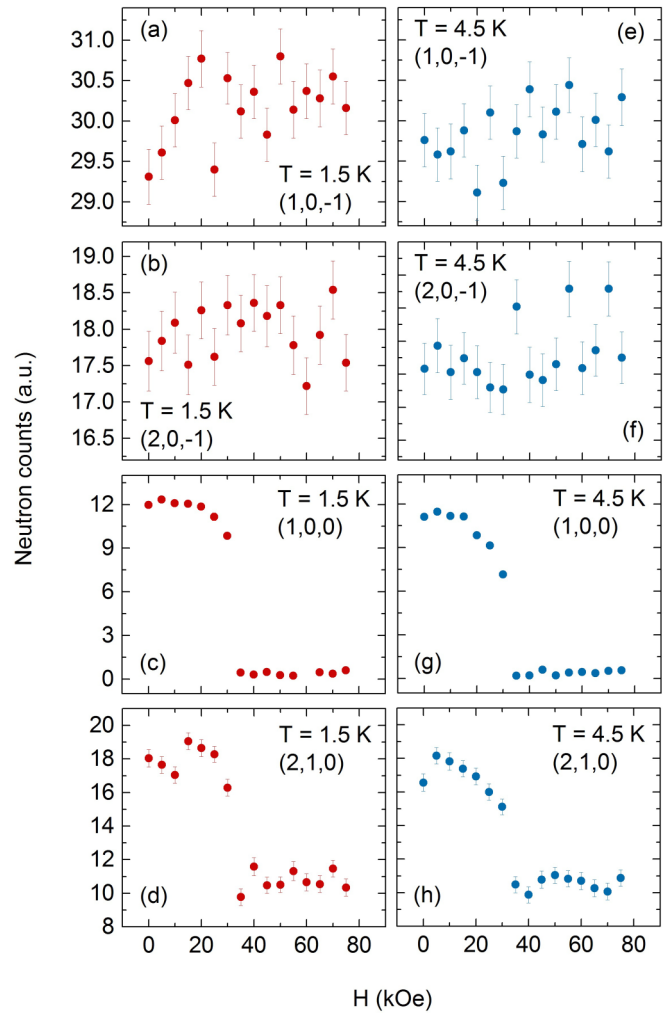

FIG. 8. Neutron counts at the peak maximum versus magnetic field at 1.5 K (left) and 4.5 K (right) for different types of Bragg reflections that are site specific in the second and fourth IRs for their magnetic contribution.

the c axis, our magnetization and neutron diffraction data are compatible with a spin flip of the Yb^{3+} ($2a$) moments that become aligned with the field and with the Yb^{3+} ($4b$) magnetic moments. This correlates well with the observed steplike change in the electric polarization accompanying the field-induced magnetic transition. These polarization changes could originate from small alterations in the atomic/electronic positions due to spin-lattice coupling together with a change in Yb-Mn and Yb-Yb magnetic interactions.

The H-T phase diagram described above is consistent with the SHG results and very similar to the one reported for the h-$ErMnO_3$ compound [34]. It has been rationalized phenomenologically through the Landau theory of phase transition [35]. An important microscopic parameter seems to be the Mn-rare-earth coupling. In the present study, it is evidenced through the polarization of the Yb^{3+} ($4b$) moments by the Mn^{3+} ones and through the reorientation of the Mn^{3+} moments triggered by the Yb^{3+} ($2a$) magnetic ordering. This coupling also has signatures in the dynamical properties of $YbMnO_3$ [33,36,37], whereas it confers its electroactivity to a magnon in $ErMnO_3$ [38]. A puzzling issue remains in the mutual orthogonal orientation of the Mn^{3+} and Yb^{3+} magnetic moments which excludes a coupling mechanism by isotropic exchange interactions and calls for subtler mechanisms. The deviation of the x_{Mn} coordinate from 1/3 has also been proposed as an important parameter in the selection of the Mn^{3+} magnetic configuration, either by triggering the sign of the interlayer Mn^{3+} magnetic effective interaction [31] or by determining the orientation of Mn^{3+} within the (a, b) plane through spin-lattice coupling [39]. In our study, this parameter does not seem to vary significantly with the temperature, impeding a definite conclusion on this issue.

ACKNOWLEDGMENTS

This work was partly supported by the French ANR Project DYMAGE (ANR-13-BS04-0013) and by the HLD at HZDR, a member of the European Magnetic Field Laboratory (EMFL). D.Z.D. gratefully acknowledges the financial support by the project DN - 08/9 of the Bulgarian Science Fund. The work of M.I.A. was supported by the government of the Basque Country (Project No. IT779-13) and the Spanish Ministry of Economy and Competitiveness and FEDER funds (Project No. MAT2015-66441-P). A.A.M. and V.Yu.I. gratefully acknowledge the financial support from the program of the Russian Academy of Sciences "Actual problems of low temperature physics."

[1] E. F. Bertaut, F. Forrat, and P. Fang, Compt. Rend. Acad. Sci. (Paris) **256**, 1958 (1963).
[2] B. B. van Aken, T. T. M. Palstra, A. Filippetti, and N. A. Spaldin, Nat. Mater. **3**, 164 (2004).
[3] C. J. Fennie and K. M. Rabe, Phys. Rev. B **72**, 100103 (2005).
[4] S. Lee, A. Pirogov, M. Kang, K.-H. Jang, M. Yonemura, T. Kamiyama, S.-W. Cheong, F. Gozzo, N. Shin, H. Kimura, Y. Noda, and J.-G. Park, Nature (London) **451**, 805 (2008).
[5] M. Lilienblum, T. Lottermoser, S. Manz, S. Selbach, A. Cano, and M. Fiebig, Nat. Phys. **11**, 1070 (2015).
[6] H. Sim, J. Oh, J. Jeong, M. Duc Le, and J.-G. Park, Acta Crystallogr., Sect. B **72**, 3 (2016).
[7] D. Bansal, J. L. Niedziela, R. Sinclair, V. O. Garlea, D. L. Abernathy, S. Chi, Y. Ren, H. Zhou, and O. Delaire, Nat. Commun. **9**, 15 (2018).
[8] H. Sim, J. Jeong, H. Kim, S.-W. Cheong, and J.-G. Park, J. Phys.: Condens. Matter **30**, 105601 (2018).
[9] S. H. Skjærvø, Q. N. Meier, M. Feygenson, N. A. Spaldin, S. J. L. Billinge, E. S. Bozin, and S. M. Selbach, arXiv:1707.09649.
[10] H. Sugie, N. Iwata, and K. Kohn, J. Phys. Soc. Jpn. **71**, 1558 (2002).
[11] N. Hur, I. K. Jeong, M. F. Hundley, S. B. Kim, and S. W. Cheong, Phys. Rev. B **79**, 134120 (2009).
[12] P. J. Brown and T. Chatterjy, J. Phys.: Condens. Matter **18**, 10085 (2006).
[13] J. Fontcuberta, M. Gospodinov, and V. Skumryev, J. Appl. Phys. **103**, 07B722 (2008).
[14] X. Fabrèges, I. Mirebeau, P. Bonville, S. Petit, G. Lebras-Jasmin, A. Forget, G. André, and S. Pailhès, Phys. Rev. B **78**, 214422 (2008).
[15] M. Fiebig, D. Fröhlich, K. Kohn, St. Leute, Th. Lottermoser, V. V. Pavlov, and R. V. Pisarev, Phys. Rev. Lett. **84**, 5620 (2000).
[16] M. Fiebig, Th. Lottermoser, and R. V. Pisarev, J. Appl. Phys. **93**, 8194 (2003).
[17] U. Adem, M. Mostovoy, N. Bellido, A. A. Nugroho, C. Simon, and T. T. M. Palstra, J. Phys.: Condens. Matter **21**, 496002 (2009).
[18] G. Qiang, Y. Fang, X. Lu, S. Cao, and J. Zhang, Appl. Phys. Lett. **108**, 022906 (2016).
[19] F. Yen, C. R. de la Cruz, B. Lorenz, E. Galstyan, Y. Y. Sun, M. M. Gospodinov, and C. W. Chu, J. Mater. Res. **22**, 2163 (2007).
[20] Z. J. Huang, Y. Cao, Y. Y. Sun, Y. Y. Xue, and C. W. Chu, Phys. Rev. B **56**, 2623 (1997).
[21] E. F. Bertaut, Acta Crystallogr., Sect. A **24**, 217 (1968).
[22] A. Muñoz, J. A. Alonso, M. J. Martínez-Lope, M. T. Casáis, J. L. Martínez, and M. T. Fernández-Díaz, Phys. Rev. B **62**, 9498 (2000).
[23] V. Skumryev, M. D. Kuz'min, M. Gospodinov, and J. Fontcuberta, Phys. Rev. B **79**, 212414 (2009).
[24] N. Abramov, V. Chichkov, S. E. Lofland, and Y. M. Mukovskii, J. Appl. Phys. **109**, 07D912 (2011).
[25] A. Midya, S. N. Das, P. Mandal, S. Pandya, and V. Ganesan, Phys. Rev. B **84**, 235127 (2011).
[26] B. Lorenz, ISRN Condens. Matter Phys. **2013**, 497073 (2013).
[27] J. Rodriguez-Carvajal, Phys. B (Amsterdam, Neth.) **192**, 55 (1993).
[28] P. J. Becker and P. Coppens, Acta Crystallogr., Sect. A **30**, 129 (1974).

[29] M. Isobe, N. Kimizuka, M. Nakamura, and T. Mohri, Acta Crystallogr., Sect. C **47**, 423 (1991).
[30] B. B. van Aken, A. Meestam, and T. T. M. Palstra, Acta Crystallogr., Sect. E **57**, 164 (2001).
[31] X. Fabrèges, S. Petit, I. Mirebeau, S. Pailhès, L. Pinsard, A. Forget, M. T. Fernandez-Diaz, and F. Porcher, Phys. Rev. Lett. **103**, 067204 (2009).
[32] H. A. Salama, C. J. Voyer, D. H. Ryan, and G. A. Stewart, J. Appl. Phys. **105**, 07E110 (2009).
[33] E. C. Standard, T. Stanislavchuk, A. A. Sirenko, N. Lee, and S.-W. Cheong, Phys. Rev. B **85**, 144422 (2012).
[34] D. Meier, H. Ryll, K. Kiefer, B. Klemke, J.-U. Hoffmann, R. Ramesh, and M. Fiebig, Phys. Rev. B **86**, 184415 (2012).
[35] I. Munawar and S. H. Curnoe, J. Phys.: Condens. Matter **18**, 9575 (2006).
[36] M. Diviš, J. Hölsä, M. Lastusaari, A. P. Litvinchuk, and V. Nekvasil, J. Alloys Compd. **451**, 662 (2008).
[37] J. Liu, C. Toulouse, P. Rovillain, M. Cazayous, Y. Gallais, M.-A. Measson, N. Lee, S. W. Cheong, and A. Sacuto, Phys. Rev. B **86**, 184410 (2012).
[38] L. Chaix, S. deBrion, S. Petit, R. Ballou, L.-P. Regnault, J. Ollivier, J.-B. Brubach, P. Roy, J. Debray, P. Lejay, A. Cano, E. Ressouche, and V. Simonet, Phys. Rev. Lett. **112**, 137201 (2014).
[39] I. V. Solovyev, M. V. Valentyuk, and V. V. Mazurenko, Phys. Rev. B **86**, 054407 (2012).